

Abstract

A 3-dimensional calculation of atmospheric neutrinos flux is presented, and the results are compared with those of a 1-dimensional one. In this study, interaction and propagation of particles is treated in a 3-dimensional way including the curvature of charged particles due to the geomagnetic field, which is assumed to be a dipole field. The purpose of this paper is limited to the comparison of calculation schemes. The updated flux value with new interaction model and primary flux model will be reported in a separate paper.

Except for nearly horizontal directions, the flux is very similar to the result of 1 dimensional calculations. However, for near-horizontal directions an enhancement of the neutrino flux is seen even at energies as high as 1 GeV. The production height of neutrinos is lower than the prediction by 1-dimensional calculation for near-horizontal directions, and is a little higher for near-vertical directions. However, the difference is not evident except for near-horizontal directions.

95.85.Ry, 14.60.Pq, 96.40.Tv

Comparison of 3-Dimensional and 1-Dimensional Schemes in the calculation of Atmospheric Neutrinos

M. Honda, T. Kajita

Institute for Cosmic Ray Research, University of Tokyo, Kashiwa 277-8582, Japan.

K. Kasahara

Dept. of Electronic Information Systems, Shibaura Inst. of Tech. Fukasaku, Ohmiya 330-8570, Japan.

and, S. Midorikawa

Faculty of Engineering, Aomori University, Aomori 030-0943, Japan.

(October 28, 2018)

I. INTRODUCTION:

The conflict between experimental data and the theoretical predictions of atmospheric neutrinos gives evidence for neutrino oscillations [5] (see also [1] [2] [3] [4]). The data from Super-Kamiokande, which dominate the statistics in the atmospheric neutrino data, are well explained by $\nu_\tau \leftrightarrow \nu_\mu$ oscillation with $\Delta m^2 \simeq 3 \times 10^{-3} \text{ eV}^2$ and $\sin^2 2\theta \sim 1$. We note that the oscillation mode of $\nu_\tau \leftrightarrow \nu_\mu$ with $\Delta m^2 \sim 1 \times 10^{-2} \text{ eV}^2$ was suggested [8] [9] [10] immediately after the discovery of the atmospheric neutrino anomaly [6], using the the atmospheric neutrinos flux predicted in the 1-dimensional approximation [7]. The theoretical study of the atmospheric neutrinos has also been improved since that time, but most of them still employ the 1-dimensional approximation [12] [11]. For further study of neutrino oscillations, a better prediction of the atmospheric neutrino flux calculated using a 3-dimensional scheme may be needed.

The ‘3D-effects’ are not so large; the bending of muons in the geomagnetic field is ~ 0.1 radian (~ 5 degree) in the average muon lifetime, and the transverse momentum of a secondary particle in a hadronic interaction is typically $0.3 \text{ GeV}/c$. Both are small effects for neutrinos with energy of $\gtrsim 1 \text{ GeV}$, and could be ignored for $\gg 1 \text{ GeV}$. Therefore it is considered that 1-dimensional calculation is sufficient for the confirmation of neutrino oscillation and their nonzero masses. The effects become important, however, for neutrinos with energies $\lesssim 1 \text{ GeV}$.

One of the difficult problems of the 3-dimensional calculation is the computation time. If we sample the cosmic ray uniformly over the surface of the Earth, roughly speaking, only $(\text{Detector-size}/\text{Earth-radius})^2$ of the produced neutrinos go through the detector. The 3-dimensional calculations that have been reported so far adopt some ideas which address this computation problem. Tserkovnyak et al. assumed a huge detector size [14]. However, they still suffered from small statistics. On the other hand, Battistoni et al. assumed a spherical symmetry ignoring the geomagnetic field in the air [13], and they found an enhancement of atmospheric neutrino fluxes in near-horizontal directions at low energies. This is a general

feature in the 3-dimensional calculation, as Lipari gives an explanation of it in terms of geometry [15]. Such a feature is not seen in the 1-dimensional calculation.

In this study, we introduce a dipole geomagnetic field both for the geomagnetic cutoff test and particle simulation in the air. With the axisymmetry of the dipole geomagnetic field, we can integrate the results over longitudinal directions and reduce the computation time to get the sufficient statistics. This dipole magnetic field may be an over simplification for the geomagnetism, but is useful to estimate the effect of the geomagnetic field in the air on atmospheric neutrinos. This is stressed by Lipari [16].

In this paper, we concentrate on the comparison of the 3-dimensional calculation, with and without the geomagnetic field in the air, and the 1 dimensional one. The flux value will be reported in a separate paper with an improved interaction model.

II. SIMULATION SETUPS AND PROCEDURE

FIGURES

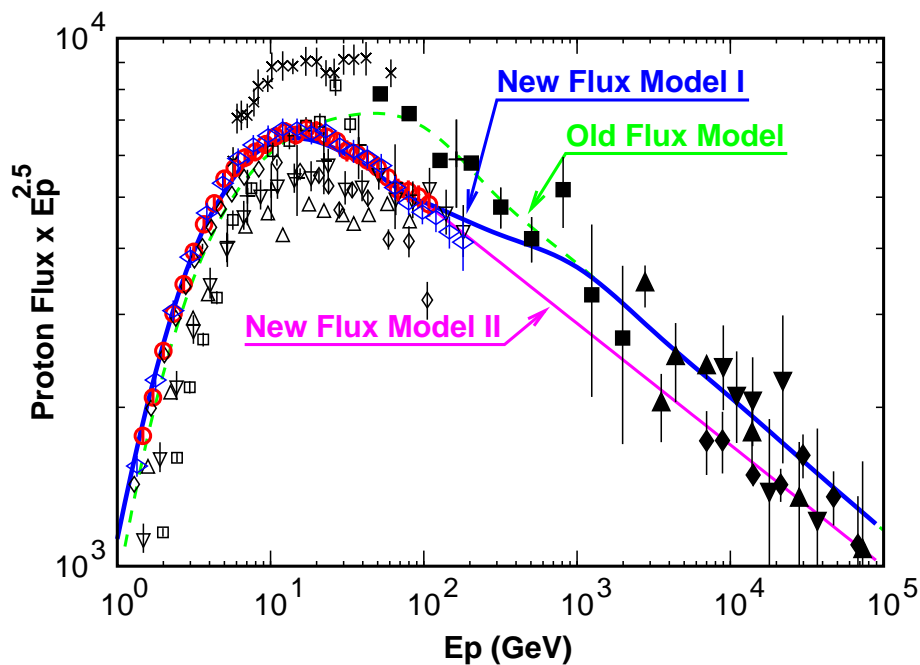


FIG. 1. Primary cosmic ray observation and our model curves for protons at solar minimum. New Flux Model I is used in this study. Crosses indicate data from Ref.[18], open squares MASS[19], open upward triangles LEAP[20], open downward triangles IMAX[21], open vertical diamonds CAPRICE[22], open circles BESS[23], and open horizontal diamonds AMS[24]. Pluses indicate data from Ref.[25] closed squares Ref.[26] closed vertical diamond JACEE[27] closed upward triangles Ref[28], and closed downward triangles Ref[29].

The atmospheric neutrino flux of $\lesssim 1$ GeV, in which we expect sizable differences between 1-dimensional and 3-dimensional calculations, is mainly produced by the cosmic rays with energies below 100 GeV. The recently observed proton cosmic ray flux in this energy region is lower than the HKKM flux model above 30 GeV, showing the maximum difference of 30 % at around 100 GeV (Fig. 1). Variations of observed flux for < 10 GeV are also seen. However, this is mainly due to modulation by Solar activity, and they agree with each other when a proper correction is applied. Therefore, we renew the primary proton flux model based on recent observations, especially those of BESS [23] and AMS [24]. Above 100 GeV, we construct two primary flux models for proton cosmic rays: New Flux Model I and New Flux Model II shown in Fig. 1 with available data. They are considered as the upper and lower bounds of plausible extrapolation from lower energies. The fraction of heavier chemical composition in cosmic rays is small at < 100 GeV, and we take the values of the old HKKM flux model for them.

As a temporary choice, we use the New Flux Model I in this study. The differences in the primary flux model, including that for heavier nuclei, would not result in large differences in the comparison of 1D and 3D calculation schemes. However, the differences in neutrino flux between the New Flux Model I, II, and the Old Flux Model are briefly addressed in a later section.

For the interaction model, we use the same interaction model as the HKKM [11] calculations in this study. We stress that, however, we are improving the interaction model,

since the combination of new flux model and present interaction model does not explain the observed flux of secondary cosmic rays at several altitudes. The updated interaction model as well as the primary flux model will be reported in a forthcoming paper with the resulting neutrino flux.

We assume that the surface of the Earth is a simple sphere with radius of $R_e \simeq 6378$ km, and use a geomagnetic coordinate system such that the center of the Earth is the origin and the line from the center of the Earth to the magnetic north pole is the z-axis. The geomagnetic field is approximated by a dipole magnetic field as,

$$B_x = B_0 \cdot 3zxR_e^3/r^5, \quad B_y = B_0 \cdot 3zyR_e^3/r^5, \quad \text{and} \quad B_z = B_0 \cdot (3z^2 - r^2)R_e^3/r^5 \quad (2.1)$$

with $B_0 = -0.30$ Gauss in this coordinate system. The position of magnetic north pole is calculated to be at (71.4W, 79.3N) for the geomagnetic field in 1995. And the magnetic latitudes for SK, Soudan-II, and SNO are 26.9 N, 58 N, and 54.0 N, respectively. The position of SK may be considered as the mid-magnetic-latitudes (MML), and that of Soudan-II and SNO as the high-magnetic-latitudes (HML).

In addition to the surface of the Earth, we consider three more spheres. The first one is called the injection sphere with the radius of $R_e + 100$ km, the second one is the simulation boundary sphere with radius of $R_e + 300$ km, and the third one is the geomagnetic sphere with radius of $10 \times R_e$. (See Fig. 2.) The simulation of cosmic rays starts at the injection sphere, and is carried out in the space between the surface of the Earth and the simulation boundary sphere. Outside of the geomagnetic sphere, we consider the cosmic rays are free from the effects of the geomagnetic field.

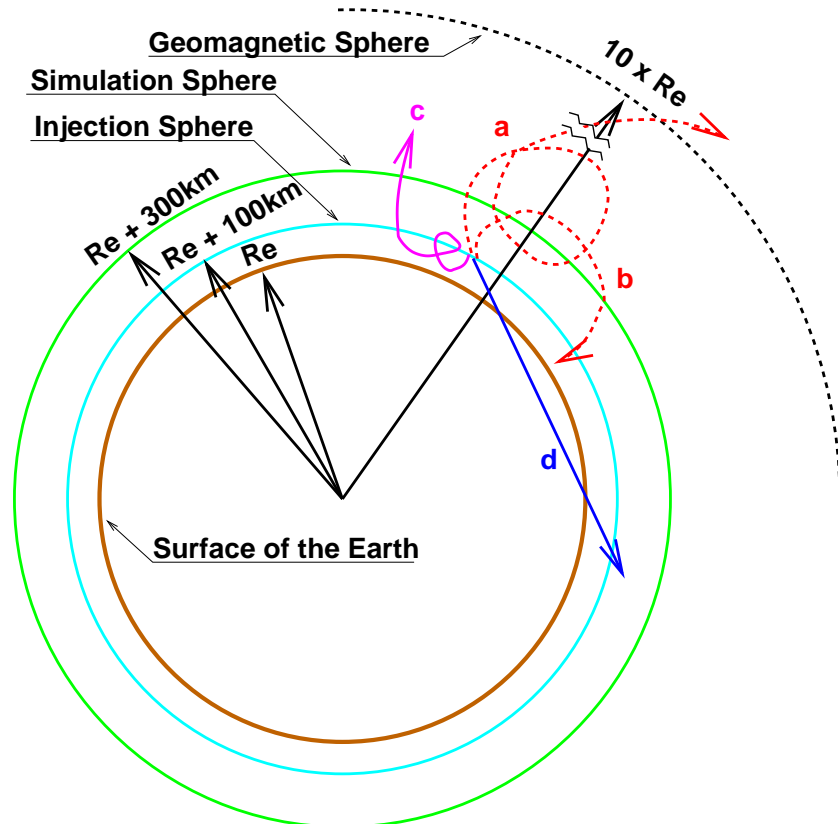


FIG. 2. Schematic view of the 3-dimensional calculation of atmospheric neutrinos. The curves in the figure show a) the backtracking orbit for an allowed path, b) same as a) but for a forbidden path, c) the orbit of a discarded particle, and d) the track for neutrinos.

First, the chemical composition and energy are sampled for a cosmic ray following the energy spectrum of each chemical composition. Then the injection position is sampled uniformly over the injection sphere and the arrival directions are sampled so that the zenith angle distribution is proportional to $[\cos\theta \cdot d\cos\theta]$, where θ is the zenith angle at the injection point. We record the sampled energy, the chemical composition, the position of the injection and the direction of the cosmic ray, irrespective of the result of the geomagnetic cutoff test.

For the geomagnetic cutoff test, we trace the backward path of a particle with the same mass and energy as the cosmic ray but with the opposite charge. If the particle goes out of the geomagnetic sphere within 100 sec without going into the injection sphere, we judge the cosmic ray has passed the geomagnetic cutoff. The above geomagnetic cutoff test only picks up cosmic rays which arrive in the injection plane for the first time. Note that the geomagnetic cutoff test works exactly the same way for two particles with the same rigidity (p/Z).

The cosmic rays which pass the geomagnetic cutoff test are fed into Cosmos simulation code [17]. When a neutrino is produced in the simulation, the production position and the direction are recorded. Other particles are traced until they decay, they leave the simulation sphere or enter the Earth.

For the neutrinos, we calculate both the point of entrance into the Earth and the point of emergence from the Earth; neutrinos which do not enter the Earth are discarded. At each point, the arrival zenith angle and the azimuth angles are calculated. We note that the arrival zenith angle is defined as the angle between the downward normal vector direction and direction of the neutrino at each point. The azimuth angle is defined as the projection angle on the tangential plane at each point.

We refer to the calculation setup explained in the above as the 3D calculation. We performed three other calculations with different setups to the above. The first is a 1-dimensional calculation such that the geomagnetic cutoff test is applied with the same dipole magnetic field as in the 3-dimensional case, but all particles are treated by Cosmos in a 1-dimensional fashion (1D calculation), in which all secondary particles are produced in the direction of the primary cosmic ray. The second is such that the geomagnetic cutoff and the interaction are treated in the same way as the 3D calculation but the effect of the geomagnetic field is ignored in the air (3D-nomag calculation). The third is another 1D calculation such that most of procedures are the same as the 1D, but the the geomagnetic cutoff is applied with the multi-pole expanded (8th order) geomagnetic field (1D-multipole calculation). This is almost the same as the HKKM calculation [11] except for the Flux model. The New Flux Model I is used for all the above calculations. These calculations are performed both for the SK site and for North America.

III. SIMULATION RESULTS

A. Direction averaged flux

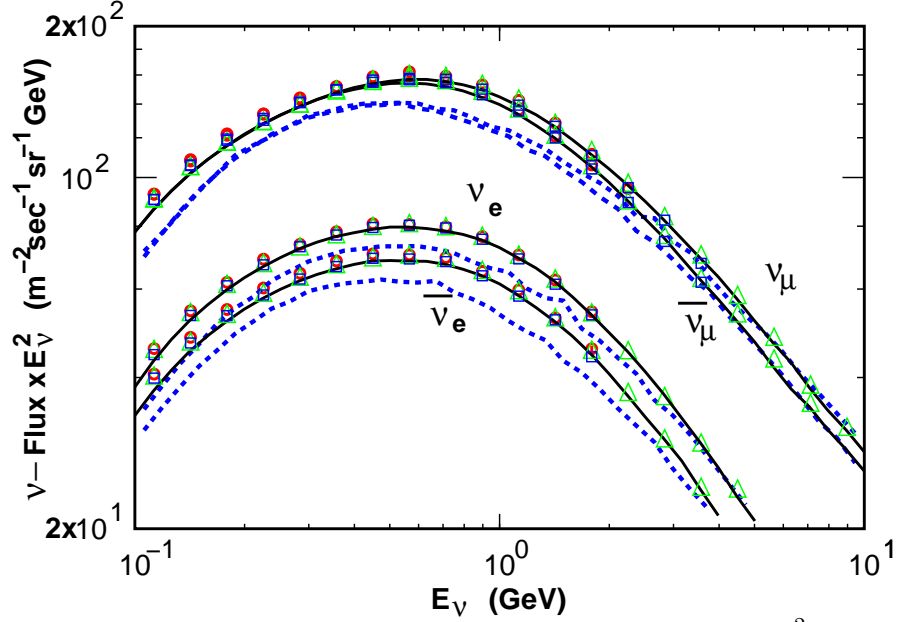


FIG. 3. Direction averaged atmospheric neutrino flux multiplied by E_ν^2 for the MML. The squares are for 3D, triangles for 1D, and circles for 3D-nomag calculations. The solid and dashed lines show the neutrino fluxes of 1D-multipole and Battistoni et al. [13] respectively.

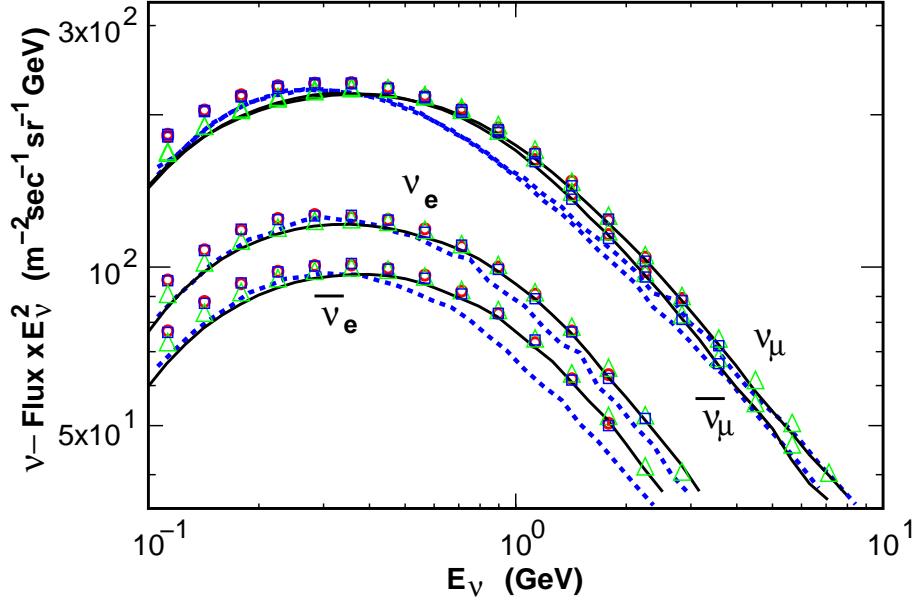


FIG. 4. Direction averaged atmospheric neutrino flux multiplied by E_ν^2 for the HML. The squares are for 3D, triangles for 1D, and circles for 3D-nomag calculations. The solid and dashed lines show the neutrino fluxes of 1D-multipole and Battistoni et al. [13] respectively.

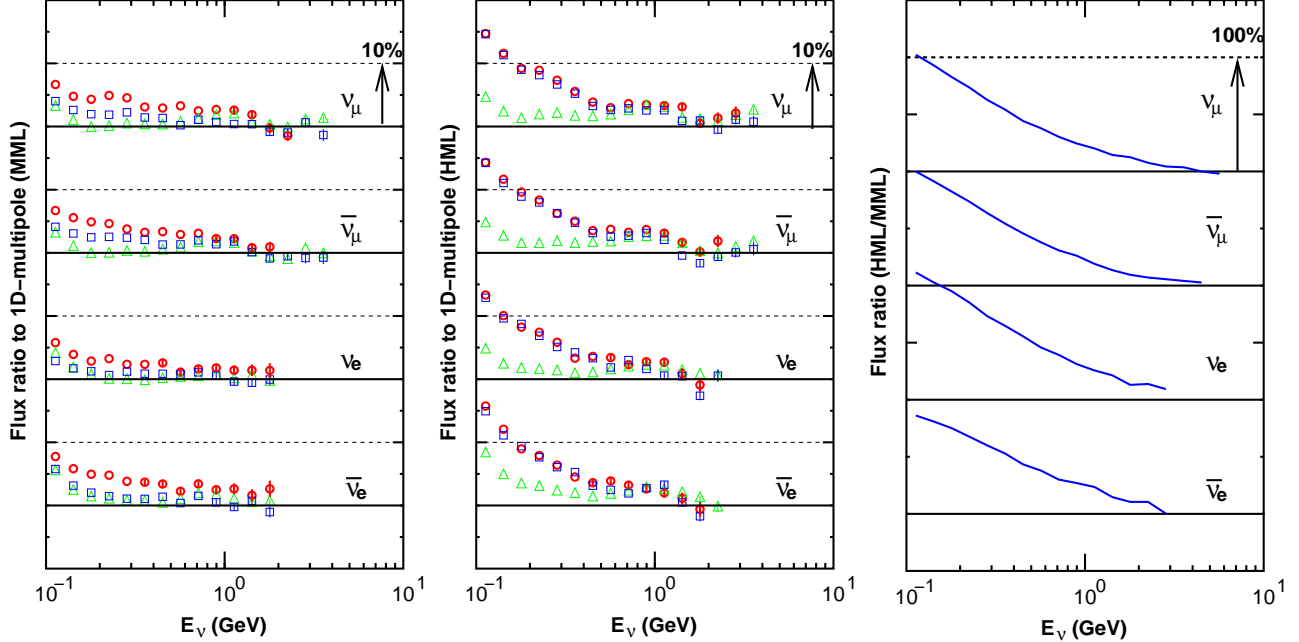


FIG. 5. Flux ratios of 1D, 3D, and 3D-nomag to the 1D-multipole in MML(left) and HML(center), and the ratio of 3D for HML to MML (right). The squares are for 3D, triangles for 1D, and circles for 3D-nomag calculations.

In Fig. 3, we show the energy spectra averaged over all directions of atmospheric neutrinos predicted by several different calculations for the MML (mid-magnetic-latitudes), and in Fig. 4 for HML (high-magnetic-latitudes). To see the difference more clearly, we also calculated the ratios of the 1D, 3D, and 3D-nomag to the 1D-multipole fluxes for MML and HML, and the ratio of 3D fluxes for HML to that for MML in Fig. 5.

The differences between 1D, 3D, 3D-nomag, and 1D-multipole calculations using the same primary cosmic ray flux model are small for MML. The differences are less than 5 % for $\gtrsim 0.2$ GeV for all the calculation schemes, and for $\gtrsim 0.1$ GeV between 1D and 3D. On the other hand, the differences between different calculation schemes are larger in HML than those in MML.

The neutrino flux difference between the New Flux Model-I and II is $\lesssim 2 - 3$ % at 1 GeV and it grows to ~ 10 % at 10 GeV. It is rather small in the energy region where the ‘3D-effects’ are important. However, the difference between the Old Flux Model and New Flux Model-I is $8 \sim 12$ % at 1 GeV and grows to a maximum of ~ 20 % at $6 \sim 8$ GeV, and decreases above these energies.

The flux of Battistoni et al. [13] is a little smaller than ours for $\lesssim 3$ GeV, and the difference is $\sim 15\%$ at 1 GeV in MML. In HML, their flux is again smaller than ours for $0.3 \text{ GeV} \lesssim E_\nu \lesssim 3 \text{ GeV}$ ($\sim 15\%$ at 1 GeV). But below 0.3 GeV, their flux is similar or even larger than ours. However, their flux is very similar to ours at energies $\gtrsim 3$ GeV in both MML and HML.

B. Zenith angle dependence

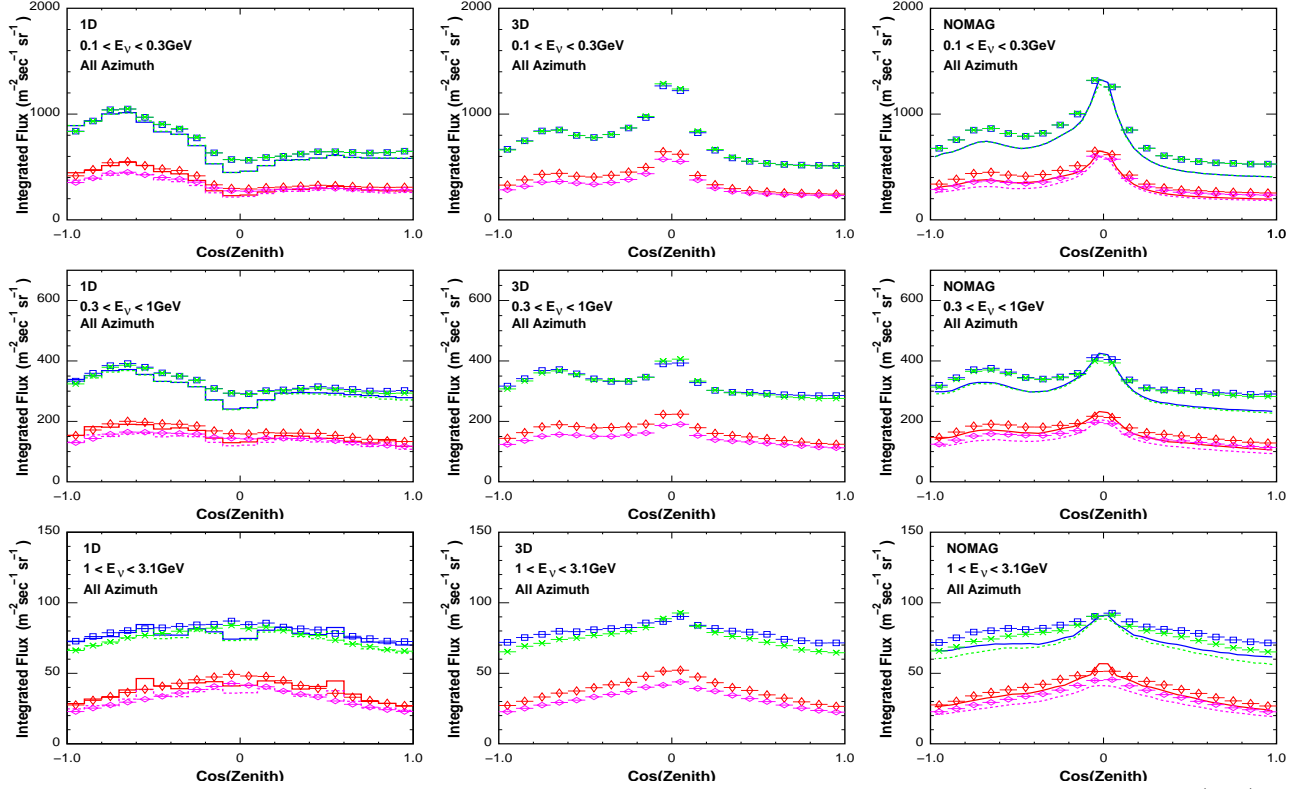


FIG. 6. Zenith angle dependence of atmospheric neutrino flux calculated in the 1D(left), 3D(center), and 3D-nomag(right) schemes for MML. Squares are for ν_μ , asterisks for $\bar{\nu}_\mu$, vertical diamonds for ν_e , and horizontal diamonds for $\bar{\nu}_e$. The solid line histograms in 1D figures show the ν fluxes, and the dotted ones the $\bar{\nu}$ fluxes for 1D-multipole calculation. The solid lines in 3D-nomag figures show the ν fluxes, and the dotted lines the $\bar{\nu}$ fluxes from Ref. [13]. The neutrino fluxes are integrated in the energy range of 0.1 – 0.3 GeV, 0.3 – 1 GeV, and 1 – 3.1 GeV, and averaged over all the azimuth angles. $\text{Cos}(\text{zenith}) = 1$ is for the downward going neutrinos. The results of 1D calculation is also plotted in the 3D figure as the solid line histogram for ν and dotted line histogram for $\bar{\nu}$ for the comparison.

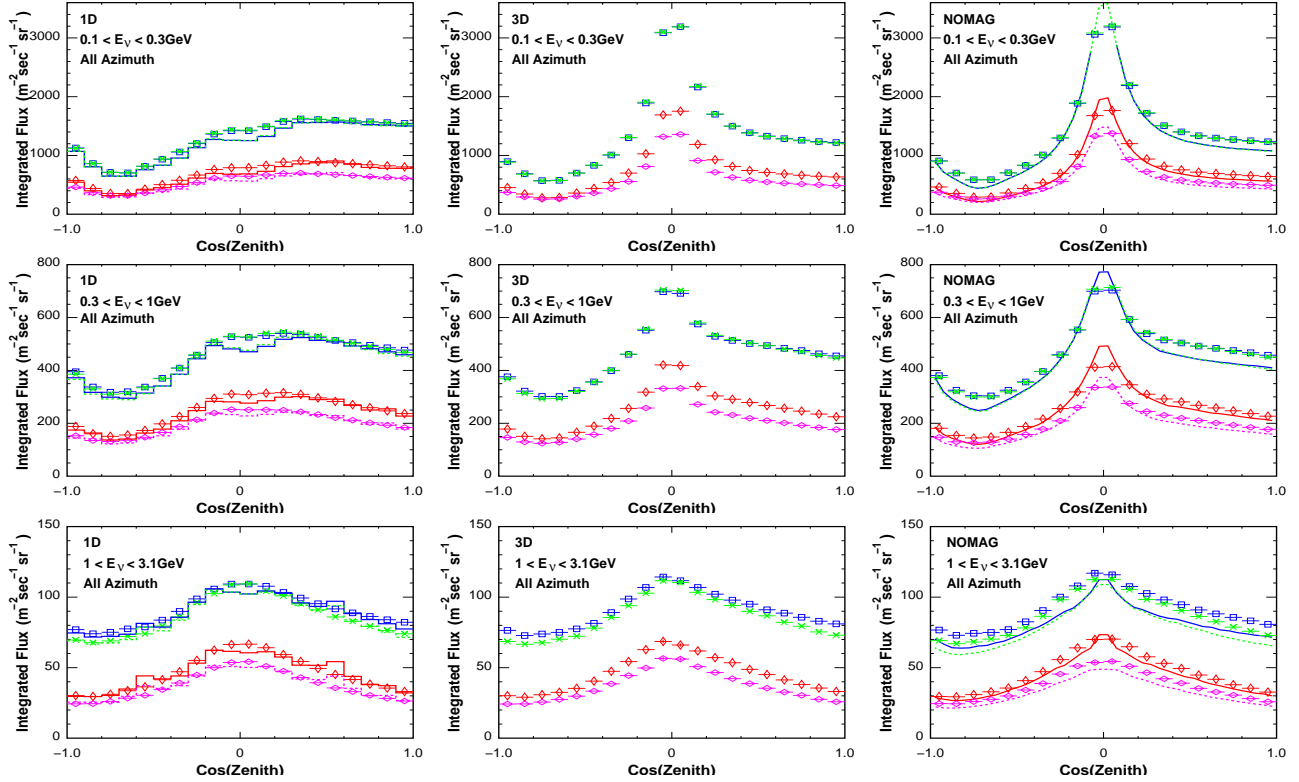


FIG. 7. Zenith angle dependence of atmospheric neutrino flux calculated in the 1D(left), 3D(center), and 3D-nomag(right) schemes for HML. Squares are for ν_μ , asterisks for $\bar{\nu}_\mu$, vertical diamonds for ν_e , and horizontal diamonds for $\bar{\nu}_e$ for 1D, 3D, and 3D-nomag calculations. The solid line histograms in 1D figures show the ν fluxes, and the dotted ones the $\bar{\nu}$ fluxes for 1D-multipole calculation. The solid lines in 3D-nomag figures show the ν fluxes, and the dotted lines the $\bar{\nu}$ fluxes from Ref. [13]. The neutrino fluxes are integrated in the energy range of 0.1 – 0.3 GeV, 0.3 – 1 GeV, and 1 – 3.1 GeV, and averaged over all the azimuth angles. $\text{Cos}(\text{zenith}) = 1$ is for the downward going neutrinos. The results of 1D calculation is also plotted in the 3D figure as the solid line histogram for ν and dotted line histogram for $\bar{\nu}$ for the comparison.

In the 1-dimensional approximation, and without the geomagnetic cutoff, we expect larger atmospheric neutrino flux for the horizontal direction than for the vertical direction. Since the average first interaction point of cosmic rays is $\sim 100 \text{ g/cm}^2$ in column density, the inclined cosmic rays produce pions in a higher altitude than the vertical ones. When π - μ decays take place in the dense air, the resulting neutrino flux is reduced, since the interaction probability of pions with the other air nuclei and the energy loss of the muons increases with the air density. Note, however, the muon energy loss is more important than the interaction probability of pions in the energy region in which we are interested ($\lesssim 1 \text{ GeV}$).

The geomagnetic cutoff modifies the zenith angle dependence of the atmospheric neutrino flux at low energies ($\lesssim 3 \text{ GeV}$). In MML, even high rigidity particles ($\gtrsim 35 \text{ GV}$) do not pass the geomagnetic cutoff test in the near-horizontal easterly directions, while relatively low rigidity particles ($\sim 11 \text{ GV}$) pass the test in the near-vertical directions. Thus the atmospheric neutrino flux for horizontal directions is lower than that for the neighboring directions, even after averaging over all azimuth angles. In HML, we expect the downward going neutrino flux is larger than the upward going neutrino flux, since averaged cutoff

rigidity is lower for down going directions.

We show the zenith angle variation calculated in the 1D, 3D, and 3D-nomag schemes in Figs. 6 and 7 for MML and HML respectively to compare the zenith angle dependence of the atmospheric neutrino flux among different calculation schemes. The neutrino fluxes are integrated in the energy range of 0.1 – 0.3 GeV, 0.3 – 1 GeV, and 1 – 3.1 GeV, and averaged over all azimuth angles.

The zenith angle variations of the atmospheric neutrino fluxes calculated in the 1D and 1D-multipole schemes are well explained by the incident angle of the primary cosmic ray and the geomagnetic cutoff as above. In the 3D and 3D-nomag calculations, however, there is a large enhancement of neutrino fluxes in the near-horizontal directions, which is not seen in the 1D and 1D-multipole calculations. This horizontal enhancement is seen in both MML and HML. The horizontal enhancement of atmospheric neutrino flux was first reported by Battistoni et al. [13], and Lipari gave an explanation in terms of geometry [15].

For the comparison with the results of Battistoni et al. [13], we plotted their results alongside our 3D-nomag results, since they considered the geomagnetic field outside the atmosphere to calculate the geomagnetic cutoff but they did not apply the geomagnetic field in the atmosphere. We found the horizontal enhancement is $\sim 10\%$ larger than ours. However, this is not considered to be the result of the difference between the multipole and dipole geomagnetic cutoff schemes. The 1D calculation gives a larger flux than the 1D-multipole at near-horizontal directions in our study. Therefore, we conclude that the larger horizontal enhancement in the results Battistoni et al. can be explained by the difference of hadronic interaction model from ours, especially that of transverse momentum of secondary pions.

C. East-West effect

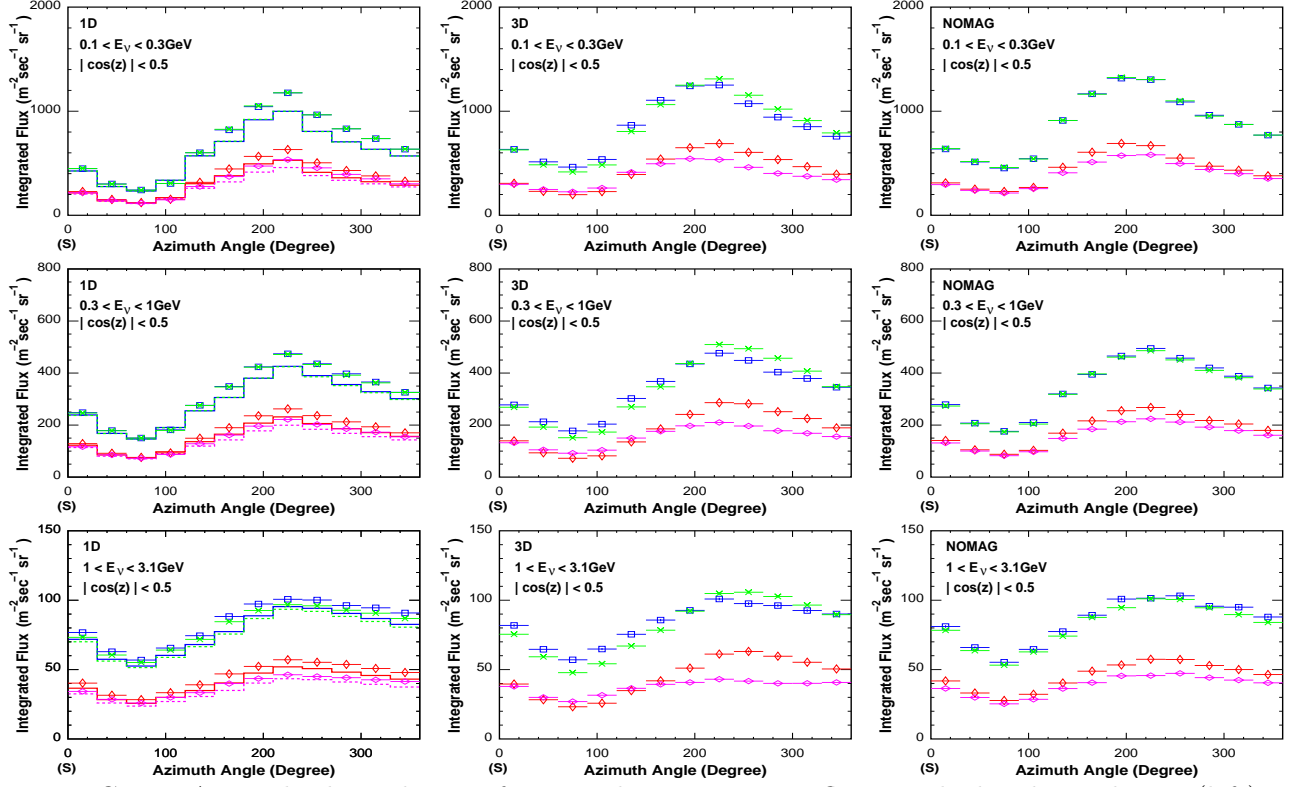


FIG. 8. Azimuth dependence of atmospheric neutrino fluxes calculated in the 1D(left), 3D(center), and 3D-nomag(right) schemes for MML. Squares are for ν_μ , asterisks for $\bar{\nu}_\mu$, vertical diamonds for ν_e , and horizontal diamonds for $\bar{\nu}_e$. The neutrino fluxes are integrated over the energy range of 0.1 – 0.3 GeV, 0.3 – 1 GeV, and 1 – 3.1 GeV, and averaged over the zenith angles: $|\cos(\theta_{\text{Zenith}})| < 0.5$. The results of 1D-multipole are plotted in 1D figures; the solid lines show the ν fluxes, and the dotted line the $\bar{\nu}$ fluxes. Azimuth = 0, 90, 180, 270, are the magnetic southerly, easterly, northerly, and westerly directions, respectively.

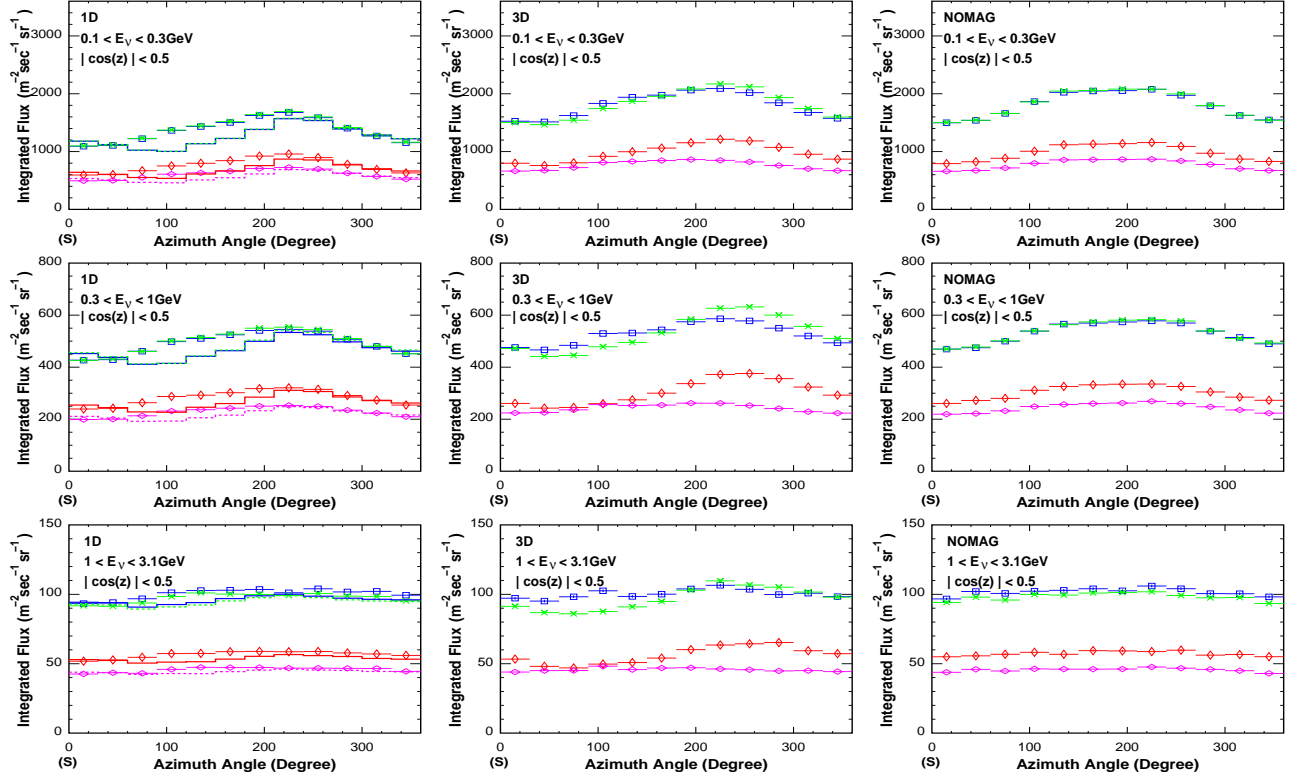


FIG. 9. Azimuth dependence of atmospheric neutrino flux calculated in the 1D(left), 3D(center), and 3D-nomag(right) procedures for HML. Squares are for ν_μ , asterisks for $\bar{\nu}_\mu$, vertical diamonds for ν_e , and horizontal diamonds for $\bar{\nu}_e$. The neutrino flux is integrated over the energy range of 0.1 – 0.3 GeV, 0.3 – 1 GeV, and 1 – 3.1 GeV, and averaged over the zenith angles: $|\cos(\theta_{\text{Zenith}})| < 0.5$. The results of 1D-multipole are plotted in 1D figures; the solid lines show the ν fluxes, and the dotted line the $\bar{\nu}$ fluxes. Azimuth = 0, 90, 180, 270, are the magnetic southerly, easterly, northerly, and westerly directions respectively.

We show the azimuth variation of the neutrino fluxes calculated in 1D, 3D, and 3D-nomag schemes in Fig. 8 and Fig. 9 for MML and HML, respectively. The azimuth variation calculated in 1D-multipole scheme is also shown with that in the 1D scheme as a histogram. The neutrino flux is integrated over the energy range of 0.1 – 0.3 GeV, 0.3 – 1 GeV, and 1 – 3.1 GeV, and averaged over the zenith angles: $|\cos(\theta_{\text{Zenith}})| < 0.5$.

The azimuthal variation of the neutrino fluxes is determined only by the geomagnetic cutoff in the 1-dimensional approximation, and we expect only a small deviation from that in the 3-dimensional schemes. (For detailed discussions, see Lipari et al. [30].) The difference between 1D, 3D, and 3D-nomag is small since they use the same geomagnetic cutoff scheme. The difference between the dipole and multi-pole geomagnetic cutoff scheme is also small. Note that there is an experimental study of the azimuth variation of the atmospheric neutrino flux [31], although the statistics in this study is small.

In both MML and HML, the atmospheric neutrinos fluxes are larger in the westerly directions ($180^\circ < \text{azimuth} < 360^\circ$) than the easterly directions ($0^\circ < \text{azimuth} < 180^\circ$) due to the lower cutoff rigidity for the westerly directions. However, the difference between the westerly direction and the easterly direction is smaller in HML than in MML. Since the corresponding energy to the cutoff rigidity is near or even lower than the pion production

threshold of cosmic rays in HML, the effect of the geomagnetic cutoff is small.

We would like to note, however, that there is a feature which is not explained by the geomagnetic cutoff only. The azimuth variation of $\bar{\nu}_\mu$ and ν_e fluxes is larger than that of ν_μ and $\bar{\nu}_e$ fluxes only in the 3D calculation, and this is not seen in other calculation schemes. The differences between ν_μ and $\bar{\nu}_\mu$, and ν_e and $\bar{\nu}_e$ are considered to result from the curvature of muons in the geomagnetic field. This feature is seen both in HML and MML.

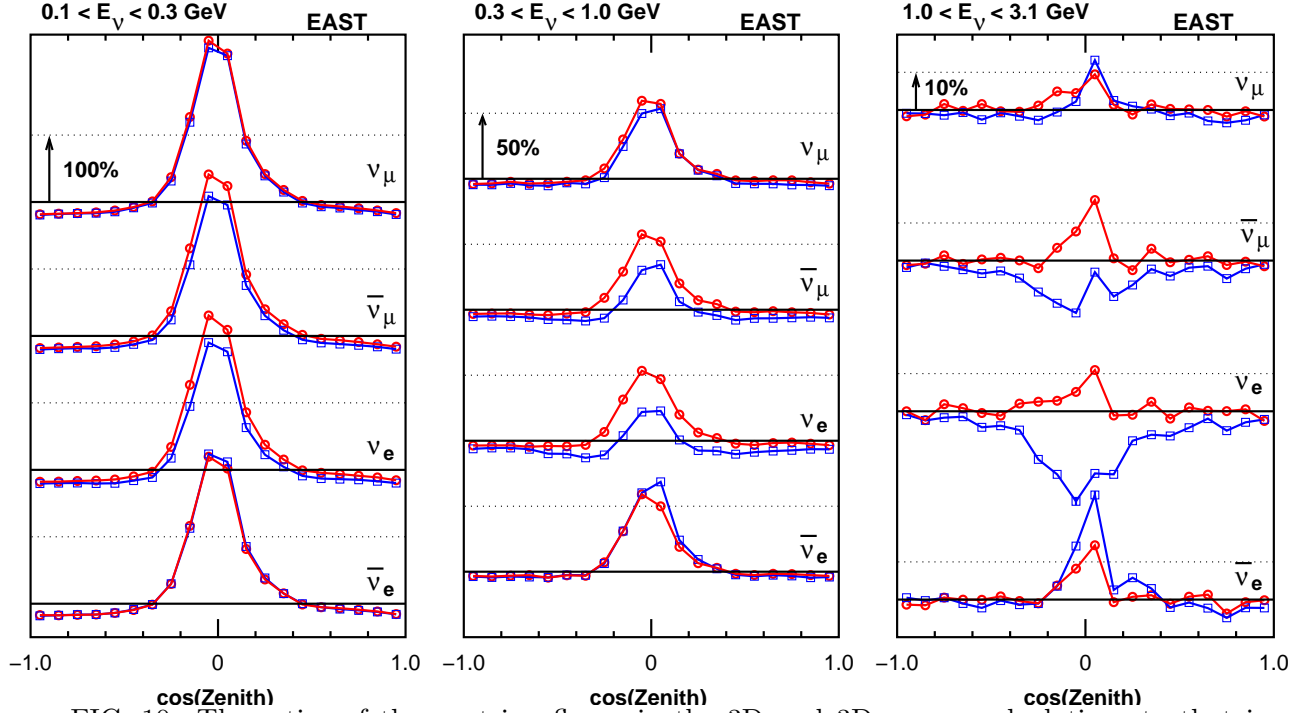


FIG. 10. The ratios of the neutrino fluxes in the 3D and 3D-nomag calculations to that in the 1D calculation for the MML for 3 energy bands: 0.1 – 0.3 GeV (left), 0.3 – 1 GeV (center), and 1 – 3.1 GeV (right) in the easterly directions, Squares indicate 3D to 1D ratios and circles 3D-nomag to 1D ratios. The scales are different for each energy band.

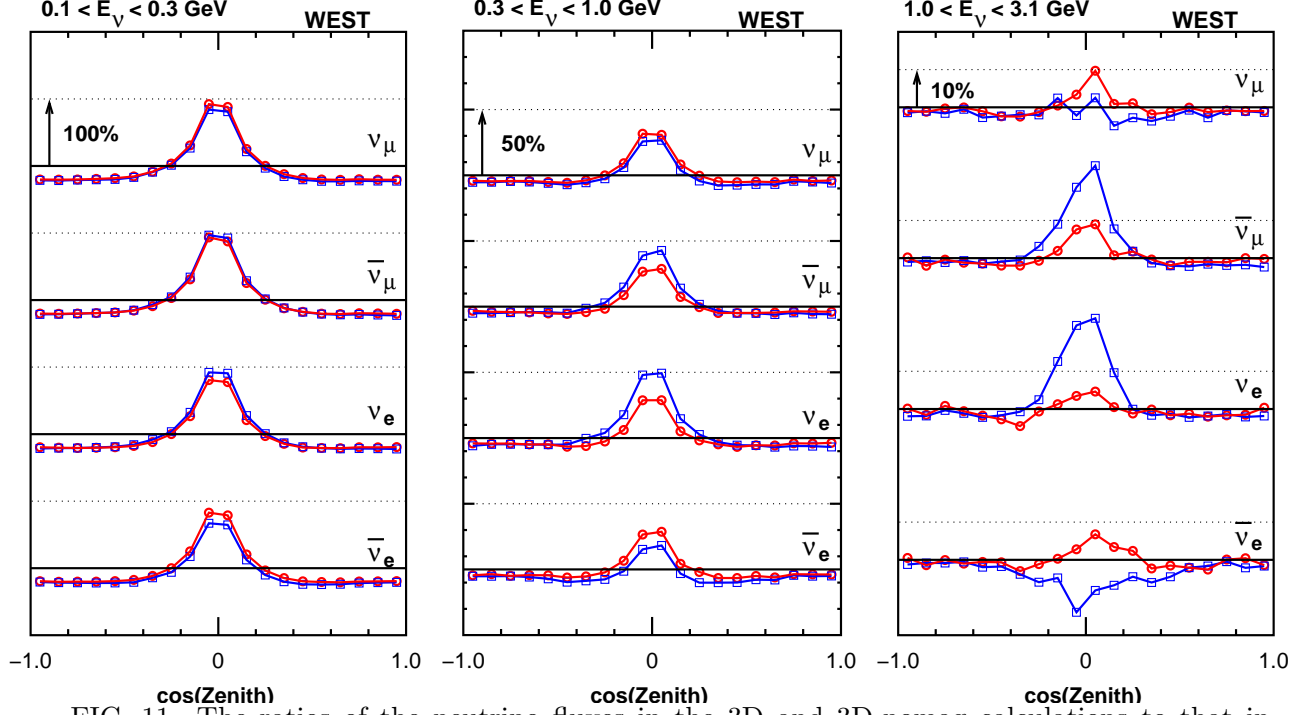


FIG. 11. The ratios of the neutrino fluxes in the 3D and 3D-nomag calculations to that in the 1D calculations for MML for 3 energy bands: 0.1 – 0.3 GeV (left), 0.3 – 1 GeV (center), and 1 – 3.1 GeV (right) in the westerly directions. Squares indicate 3D to 1D ratios and circles 3D-nomag to 1D ratios. The scales are different for each energy band.

In order to study the horizontal enhancement in more detail, we have taken the flux ratio between the 3D and 3D-nomag calculations and the 1D calculation for MML. The flux ratio is shown separately in Fig. 10 for easterly directions (S-E-N 180° in azimuth angle), and in Fig. 11 for westerly directions (N-W-S 180° in azimuth angle). Note that the unit of the vertical axis is different in these ratio-figures.

Firstly, the amplitude of the horizontal enhancement is different in easterly and westerly directions for both 3D and 3D-nomag calculations. In the near-horizontal easterly directions, it is $\sim 200\%$ for 0.1 – 0.3 GeV, and $\sim 50\%$ for 0.3 – 1.0 GeV, while in the westerly directions, it is $\sim 100\%$ for 0.1 – 0.3 GeV, and $\sim 30\%$ for 0.3 – 1 GeV. The large amplitude of the horizontal enhancement for easterly direction is caused by the low neutrino flux in 1D calculation in near-horizontal easterly directions due to the high cutoff rigidity ($\gtrsim 35\text{GV}$). The ‘3D effects’ work to smear out such a quick variation, and the ratio of the 3D flux to 1D one is larger for the region with higher cutoff rigidity if the zenith angle is the same.

In the energy range of 1.0 – 3.1 GeV, however, the horizontal enhancement becomes small and the difference between 3D and 3D-nomag calculation becomes apparent. In the 3D calculation, ν_μ and $\bar{\nu}_e$ fluxes are enhanced, while $\bar{\nu}_\mu$ and ν_e fluxes are suppressed for easterly horizontal direction, and $\bar{\nu}_\mu$ and ν_e fluxes are enhanced, while ν_μ and $\bar{\nu}_e$ fluxes are suppressed for westerly horizontal direction. These feature is not seen in the 3D-nomag calculation. Remember the fact that both the $\bar{\nu}_\mu$ and ν_e are produced in a μ^+ decay, while both the ν_μ and $\bar{\nu}_e$ are produced in a μ^- decay. These enhancement and suppression are related to the muon curvature in the geomagnetic field.

A muon is produced in a direction following the P_t distribution of pions in the hadronic

interaction of the parent cosmic ray. The directions of the potential parent cosmic rays of a muon distributed in an axisymmetric distribution around the muon direction at the muon production point, ignoring the bending of pions in the geomagnetic field. For near-horizontal muons, therefore, some of the potential parent cosmic rays are shaded by the Earth. Since a muon changes its direction by $\sim 5^\circ$ within the average life time in the geomagnetic field, the shading of the cosmic ray by the Earth works differently depending on the direction and charge of muons. For an easterly μ^+ and westerly μ^- , the shading by the Earth works more effectively, and the neutrinos produced by these muons are suppressed. For easterly μ^- and westerly μ^+ , the shading by the Earth works less effectively, and the neutrinos produced by these muons are enhanced. Note, the shading by the Earth reduces the neutrino flux near the horizontal directions, but is not seen in the resulting neutrino flux due to the large horizontal enhancement.

There is an additional effect related to the geomagnetic cutoff. The geomagnetic cutoff applied to the parent cosmic ray is different between 3D and 3D-nomag calculations due to the muon curvature. Generally speaking, a higher cutoff rigidity is applied to a μ^+ , and a lower rigidity cutoff is applied to a μ^- irrespective of direction. However, this effect is not evident except for the easterly and near-horizontal directions, where the cutoff rigidity rapidly increases toward the horizontal direction.

The amplitudes of the enhancement or suppression in the geomagnetic field are $\sim 5\%$ for the ν_μ , and $\sim 10\%$ for the $\bar{\nu}_\mu$, $20 \sim 30\%$ for ν_e and $10 \sim 20\%$ for $\bar{\nu}_e$, over a wide energy range in the near-horizontal, westerly or easterly directions. These amplitudes could be understood by the muon curvature effect explained above. Note Lipari pointed the importance of the magnetic field after the geomagnetic cutoff in Ref. [16].

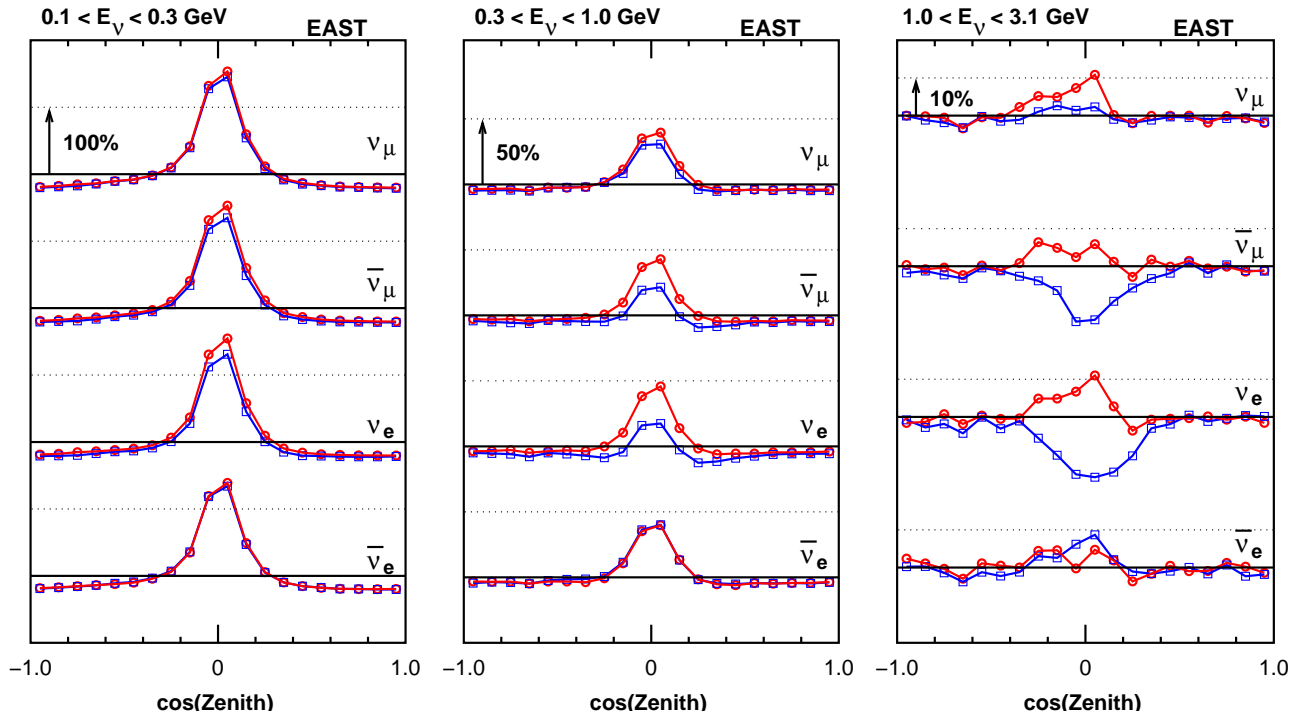


FIG. 12. The ratios of the neutrino fluxes in the 3D and 3D-nomag calculations to that in the 1D calculation for the HML for 3 energy bands: 0.1 – 0.3 GeV (left), 0.3 – 1 GeV (center), and 1 – 3.1 GeV (right) in the easterly directions. Squares indicate 3D to 1D ratios and circles 3D-nomag to 1D ratios. The scales are different for each energy band.

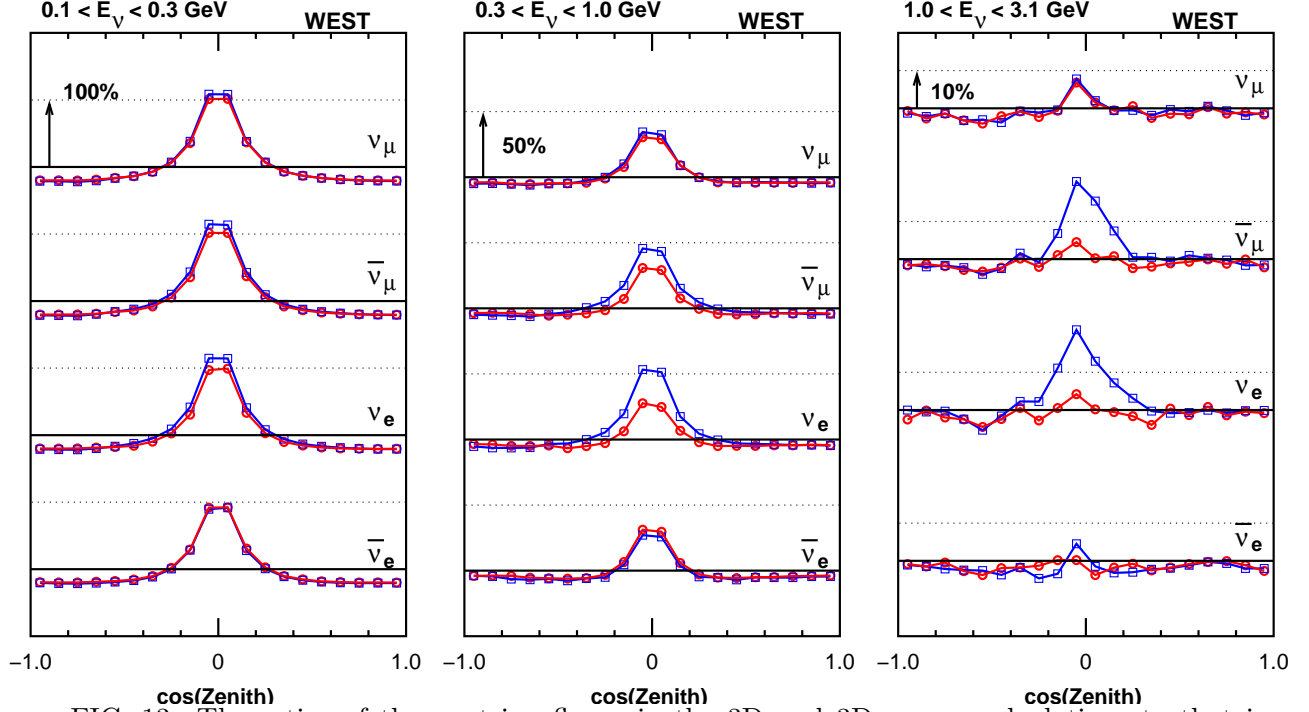


FIG. 13. The ratios of the neutrino fluxes in the 3D and 3D-nomag calculations to that in the 1D calculation for the HML for 3 energy bands: 0.1 – 0.3 GeV (left), 0.3 – 1 GeV (center), and 1 – 3.1 GeV (right) in the westerly directions. Squares indicate 3D to 1D ratios and circles 3D-nomag to 1D ratios. The scales are different for each energy band.

For the HML, the flux ratio is also calculated and shown separately in Fig. 12 for easterly directions (S-E-N 180° in azimuth angle), and Fig. 13 for westerly directions (N-W-S 180° in azimuth angle). Note that the unit of the vertical axis is different in these ratio-figures.

The general feature is the same as in the MML, but the horizontal enhancement is larger for lower neutrino energies, and the difference between 3D and 3D-nomag calculation is seen in near-horizontal directions for $\gtrsim 1$ GeV. However, the difference between easterly and westerly directions is smaller than that in the MML, since the effect of rigidity cutoff is small even in the near-horizontal directions. It is $\sim 100\%$ for 0.1 – 0.3 GeV, and $\sim 30\%$ for 0.3 – 1 GeV for both directions. Also the differences of the fluxes in 3D and 3D-nomag calculation are similar to those in MML, but a little smaller.

D. Neutrino Production Height

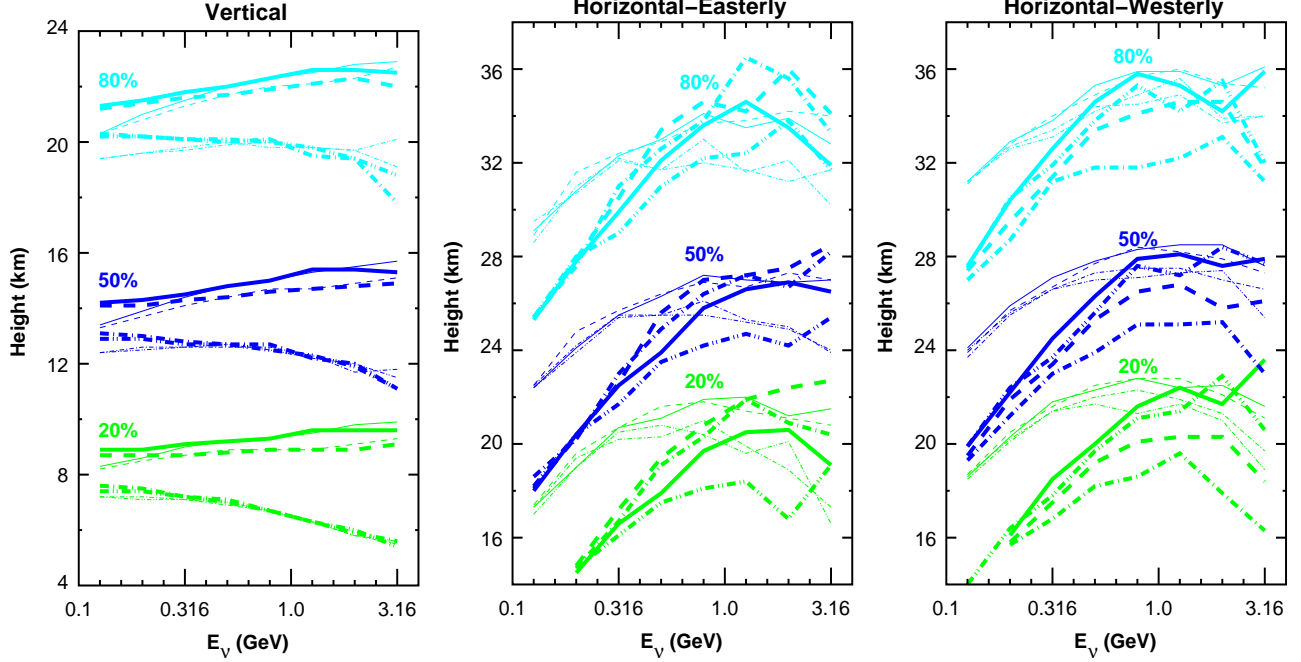


FIG. 14. Constant accumulation probability line for neutrino production height for near-vertical ($\cos(\text{zenith}) > 0.9$) (left), near-horizontal ($|\cos(\text{zenith})| < 0.1$) easterly (center), and near-horizontal westerly (right) directions for MML. Thick solid lines are for ν_μ , thick dashed lines for $\bar{\nu}_\mu$, thick dash-dotted lines for ν_e , and thick dash-double-dotted lines for $\bar{\nu}_e$ by the 3D calculation. Thin solid lines are for ν_μ , thin dashed lines for $\bar{\nu}_\mu$, thin dash-dotted lines for ν_e , and thin dash-double-dotted lines for $\bar{\nu}_e$ by the 1D calculation.

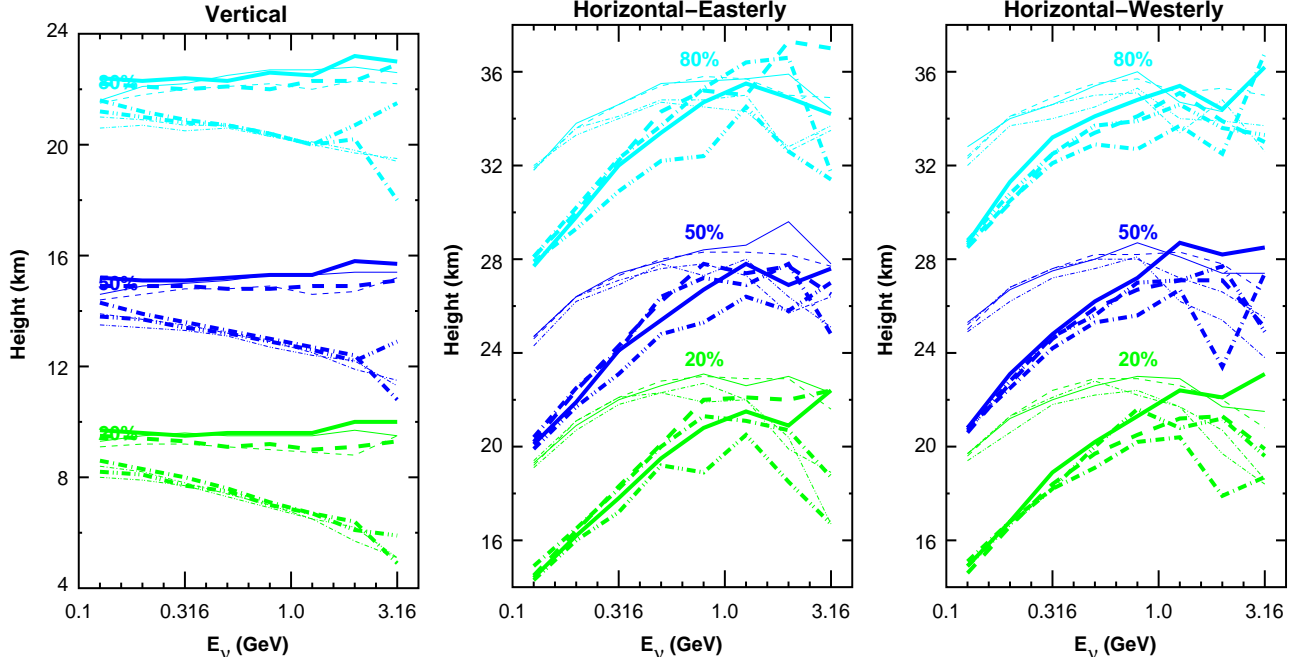


FIG. 15. Constant accumulation probability line for neutrino production height for near-vertical ($\cos(\text{zenith}) > 0.9$) (left), near-horizontal ($|\cos(\text{zenith})| < 0.1$) easterly (center), and near-horizontal westerly (right) directions for HML. Thick solid lines are for ν_μ , thick dashed lines for $\bar{\nu}_\mu$, thick dash-dotted lines for ν_e , and thick dash-double-dotted lines for $\bar{\nu}_e$ by the 3D calculation. Thin solid lines are for ν_μ , thin dashed lines for $\bar{\nu}_\mu$, thin dash-dotted lines for ν_e , and thin dash-double-dotted lines for $\bar{\nu}_e$ by the 1D calculation.

As we have already discussed in section III B, the production height of atmospheric neutrinos is mainly determined by the zenith angle of incoming cosmic rays in the 1D calculation. The cutoff rigidity also gives an additional effect to the production height for low energy neutrinos. The production height of a fixed energy neutrino is lower for higher energy parent cosmic rays, since the interaction-decay cascade extends deeper into the atmosphere when it is initiated by higher energy cosmic rays. The production height is also different for different kinds of neutrino. It is lower for ν_e and $\bar{\nu}_e$ than for ν_μ and $\bar{\nu}_\mu$, because the former are mainly produced only in the decay of muons and the latter are produced both in the muon and pion decays, and the muons are mainly produced in the pion decay.

In order to study the difference of the production height between the 1D and 3D calculations, we integrate it from ground level to the top of the atmosphere for the 1D and 3D calculations. We show the accumulated probabilities of 20 %, 50 % (median), and 80 % in Figs. 14 and 15.

We find that the production heights in the 3D and 1D calculations are almost identical for the near-vertical directions. Also they roughly agree each other for the near-horizontal directions at high energies ($\gtrsim 1$ GeV). However, the production height in the 3D calculation is apparently lower than that in the 1D calculation for near-horizontal direction and neutrino energies < 1 GeV. Despite of this difference, the essential discussions for the production height in the 1D calculation can be applied to the 3D calculation. The production height for near-vertical direction is lower than that for near-horizontal direction. Also the effect

of geomagnetic cutoff on the production height can be seen in the comparison of MML and HML, and in the comparison for easterly and westerly near-horizontal directions.

From these figures, we find that the neutrino production heights calculated in the 1D and 3D calculations agree with each other for $> 0.3\text{GeV}$ in near-vertical direction, and for $> 1\text{GeV}$ in near-horizontal directions. Note that at high energies ($\gtrsim 2\text{ GeV}$), our calculation also suffers from small statistics. However, in the near-horizontal direction and for $< 1\text{ GeV}$, the production height is lower in the 3D calculation than that in the 1D calculation. The difference of the production height between the decay products of μ^- (ν_μ and $\bar{\nu}_e$) and those of μ^+ ($\bar{\nu}_\mu$ and ν_e) is also seen in the 3D calculation in the energies of $\gtrsim 0.3\text{ GeV}$. The production height of ν_μ or $\bar{\nu}_e$ is higher than that of $\bar{\nu}_\mu$ or ν_e for westerly direction, and the production height of ν_μ or $\bar{\nu}_e$ is lower than that of $\bar{\nu}_\mu$ or ν_e for easterly direction. This can be understood by the curvature of muons.

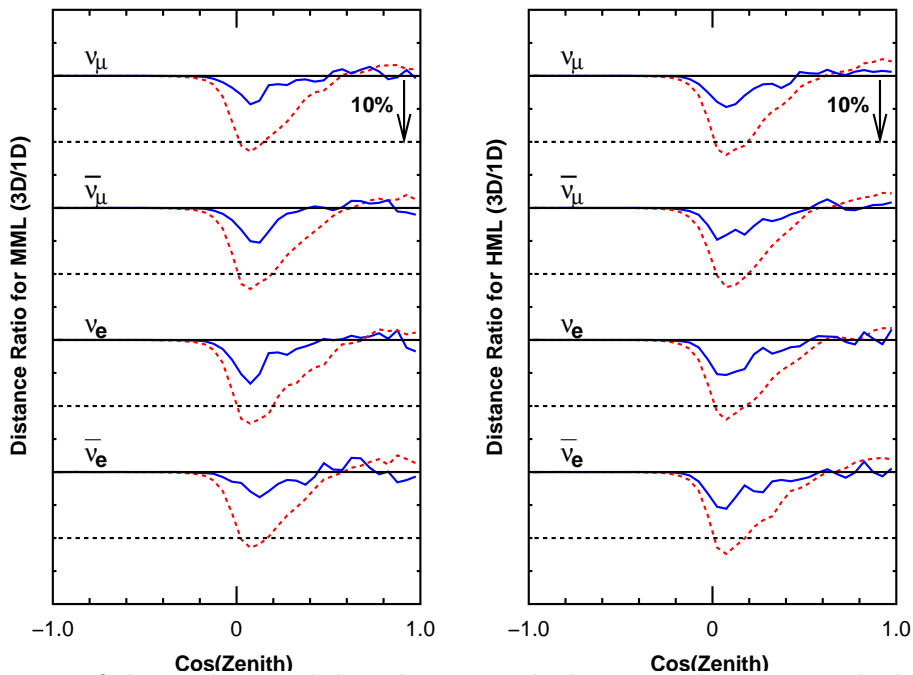


FIG. 16. Ratio of the median path length in 3D calculation to that in 1D calculation both for MML(left) and HML(right). Solid line show the ratio for 1 GeV neutrinos, and dotted line for 0.3 GeV neutrinos. $\cos\theta = 1$ denotes the downward direction for neutrinos.

Gaisser and Stanev stressed the importance of the production height and the path length in the study of neutrino oscillations [32]. We compare the path length calculated in the 1D and 3D calculations, converting the median production height to the path length by a simple relation:

$$d = \sqrt{(h^2 + 2R_e h) + (R_e \cos\theta)^2} - R_e \cos\theta \quad , \quad (3.1)$$

where h is the height, R_e is the radius of the Earth, and d is the path length. We show the ratio of the two path lengths (3D/1D) as a function of $\cos(\text{Zenith})$ in Fig. 16. In this comparison, we integrated over all the azimuth angles.

At near horizontal directions the production distance of 0.3 GeV neutrino is $\sim 10\%$ smaller for 3D calculation than for 1D at near horizontal directions. However, the difference

is small $\lesssim 5\%$ for 1 GeV neutrinos, as is expected from the comparison of production height. There is almost no difference between MML and HML in this comparison.

IV. SUMMARY AND DISCUSSIONS

We have calculated the flux of atmospheric neutrinos in a 3-dimensional scheme (3D), with the geomagnetic field simplified by a dipole approximation. We have made two other calculations using the same geomagnetic cutoff scheme: one is a 1-dimensional scheme (1D) and the other a 3-dimensional calculation without geomagnetic field in the air (3D-nomag). Adding to the above three, we have prepared another 1-dimensional calculation using the geomagnetic cutoff scheme due to a multi-pole expanded geomagnetic field similar to HKKM calculation [11] (1D-multipole).

The most remarkable fact is the large enhancement of the low energy neutrino flux at near-horizontal directions found both in the 3D and 3D-nomag calculations in both mid and high magnetic latitudes. This enhancement is already reported by other 3-dimensional calculations [13] [15], and Lipari showed that the enhancement can be explained by the geometry [15].

We introduce an explanation which is a little different to that by Lipari. We simplify the 1D-calculation; assuming that the atmospheric neutrino is produced at a fixed height h , or on a sphere with the radius of $R_e + h$. We also ignore the geomagnetic cutoff and the zenith angle dependence of production. As primary cosmic rays arrive uniformly on the sphere, the neutrino is also produced uniformly at the sphere for the downward direction. The directional distribution is proportional to

$$\cos \theta d \cos \theta dS \quad (\cos \theta > 0), \quad (4.1)$$

where θ is the zenith angle of the neutrino. Note that we take $\cos \theta > 0$ as the downward direction, and we integrate over the azimuth angles.

In the 3D calculation, the neutrino is produced in a little different direction to the primary cosmic ray direction. The directional distribution is calculated by a convolution at the production place, and proportional to

$$\int_{\cos \theta' > 0} D(\theta, \theta') \cos \theta' d \cos \theta' d \cos \theta dS. \quad (4.2)$$

where θ and θ' are the zenith angle for the neutrino in case of 3D and 1D calculations respectively, and $D(\theta, \theta')$ is a dispersion function due to the ‘3D effects’. It is important that equation 4.2 gives a non-zero value at $\cos \theta = 0$, unless $D(\theta, \theta')$ is a δ -function. The ratio of the two expressions, $\int_{\cos \theta' > 0} D(\theta, \theta') d \cos \theta' / \cos \theta$ has a divergence at $\cos \theta = 0$. The zenith angle θ is almost the same as the arrival direction at the ground, however, $\cos \theta$ never be 0 for neutrinos which is observed at ground level. The horizontal direction at the ground level actually corresponds to $\cos(\theta) = \sqrt{1 - (R_e/(R_e + h))^2}$ at the production sphere. We do not see a divergence but rather an enhancement of the neutrino flux at horizontal directions.

For neutrinos with energies > 1 GeV, $D(\theta, \theta')$ is well approximated by the δ -function. However, as long as $D(\theta, \theta')$ has a extended structure more than $\Delta\theta = 90^\circ - \cos^{-1}(\sqrt{1 - (R_e/(R_e + h))^2}) \sim 5^\circ$, a flux enhancement at horizontal directions would be seen. Thus, although ‘3D-effects’ are small, but they are enhanced by the geometry.

When we compare the 1D and 3D calculations averaging over all directions (Fig. 5), we found the difference is rather small, and 3D calculation gives $\sim 5\%$ larger than 1D even at 0.1 GeV for MML (mid-magnetic-latitudes, SK). It is also true that the the difference between the calculation with the axisymmetric dipole geomagnetic cutoff (1D) and the multipole geomagnetic cutoff (1D-multipole) is also small; 1D gives $\sim 5\%$ smaller flux than 1D-multipole calculation. Considering these facts, we would be able to conclude that the 1-dimensional calculation made in [11] is reasonably justified for the MML (mid-magnetic-latitudes, SK) as far as the average over all directions is concerned. when the neutrino flux is averaged over all directions. We note, however, this is not a general statement; the 3D calculation for the HML (high-magnetic-latitudes, Soudan-II and SNO) gives $\sim 5\%$ higher flux at 0.3 GeV and $\sim 10\%$ higher flux at 0.1 GeV. Thus, the ‘3d-effects’ work more effectively in HML than in MML, or for the position with lower cutoff rigidities.

The effect of the geomagnetic field is different for the neutrinos produced by μ^+ ($\bar{\nu}_\mu$ and ν_e) and the neutrinos produced by μ^- (ν_μ and $\bar{\nu}_e$), as is also predicted by Lipari [16]. This effect is not as large as the geometric enhancement for < 1 GeV. However, it gives $5 \sim 30\%$ effect depending on the kind of neutrinos for near-horizontal directions, and is almost independent of the neutrino energy and magnetic latitude. Since this is caused by the curvature of muons in the geomagnetic field, it would affect neutrino fluxes up to energies of $\gtrsim 10$ GeV.

The comparison of the 3D and 3D-nomag calculations in the over all direction average is also interesting. The variation of the cosmic ray shading by the muon curvature discussed in section III B works different ways in the easterly and westerly directions. We expect the difference between 3D and 3D-nomag calculations are small due to the compensation of the effect in both directions. This is true in the calculation in HML; that they agree each other within the statistical errors. In MML, however, the neutrino flux is $2 \sim 3\%$ smaller in 3D calculation than 3D-nomag at $\lesssim 0.3$ GeV even in the all direction average (Fig. 5). The coupled effect of muon curvature and geomagnetic cutoff may explain this fact, since the cutoff rigidity ($\gtrsim 10$ GV) and the effect works more effectively at MML.

The production heights of the atmospheric neutrino in the 3D calculation are similar to that in the 1D calculation for > 1 GeV. They are almost identical in the near vertical directions. In the near-horizontal directions, however, the production height in 3D calculation is lower than that in 1D calculation, and there are apparent differences in the production heights of between ν_μ and $\bar{\nu}_\mu$, and between ν_e and $\bar{\nu}_e$ due to curvature of muons in the geomagnetic field.

The path length of atmospheric neutrino is also compared in the 1D and 3D calculations, integrating all azimuth directions. The maximum difference is seen at a near horizontal direction, and is $\sim 10\%$ for 0.3 GeV neutrinos and $\sim 5\%$ neutrinos. For higher energy neutrinos ($\gg 1$ GeV), we expect very small difference between 1D and 3D calculations.

V. ACKNOWLEDGMENTS

We are grateful to P. Lipari, A. Okada, and J. Nishimura for useful discussions and comments. We thank to S. Orito and T. Sanuki for showing us the data before publication and for discussions. We also thank to C.T. Taylor for a careful reading of the manuscript.

REFERENCES

- [1] Kamiokande Collaboration: K.S. Hirata et al., Phys. Lett. B 280, 146 (1992); Y. Fukuda et al., Phys. Lett B 335, 237 (1994).
- [2] IMB collaboration: D. Casper et al., Phys. Rev. Lett 66, 2561 (1991); R. Bechker-Szendy et al., Phys. Rev. D 46, 3720 (1992).
- [3] Soudan2 Collaboration: W.W.M. Allison et al., Phys. Lett. B 446, 1562 (1999).
- [4] MACRO Collaboration: M. Ambrosio et al., Phys. Lett. B 434, 451 (1998).
- [5] The Super-Kamiokande Collaboration: Y. Fukuda et al., Phys. Rev. Lett 81, 1562 (1998).
- [6] Kamiokande Collaboration: K.S. Hirata et al., Phys. Lett B 205, 416 (1988).
- [7] T.K. Gaisser, T. Stanev, S.A. Bludman and H. Lee, Phys. Rev. Lett. 51, 223 (1983); G. Barr, T.K. Gaisser, and T. Stanev, Phys. Rev. D 39, 3532 (1989).
- [8] J.G. Learned, S. Pakvasa, and T.J. Weiler, Phys. Lett. B 207, 79 (1988).
- [9] V. Berger and K. Whisnant, Phys. Lett. B 209, 365 (1988).
- [10] K. Hidaka, M. Honda and S. Midorikawa, Phys. Rev. Lett. 61, 1537 (1988).
- [11] M. Honda, T. Kajita, K. Kahahara, S. Midorikawa, Phys. Rev. D 54, 4985 (1995),
- [12] V. Agrawal, T.K. Gaisser, P. Lipari, and T. Stanev, Phys. Rev. D 53, 1314 (1996).
- [13] G. Battistoni et al., Astropart. Phys. 12, 315 (2000).
- [14] Y. Tserkovnyak et al., hep-ph/9907450
- [15] P. Lipari, Astropart. Phys. 14, 171 (2000).
- [16] P. Lipari, Astropart. Phys. 14, 153 (2000).
- [17] K. Kasahara, Proc. of the 24th ICRC, Rome. Vol. 1, 399 (1995). See also the World-Wide-Web address;
<http://eweb.b6.kanagawa-u.ac.jp/~kasahara/ResearchHome/cosmosHome/>.
- [18] W.R. Webber et. al., 20th ICRC, Moscow vol 1, 325 (1987).
- [19] MASS Collaboration: P. Pappini, et. al., 23rd ICRC, Calgary 1, 579 (1993).
- [20] LEAP Collaboration: W.S. Seo, et. al., Astrophys. J., 378, 763 (1987).
- [21] Imax Collaboration: W. Menn, et. al., Astrophys. J., 533, 281 (2000).
- [22] CAPRICE Collaboration: G. Boezio, et. al., Astrophys. J., 518, 457, (1999).
- [23] BESS Collaboration: T. Sanuki et al., Astrophys. J., 545, 1135 (2000).
- [24] AMS Collaboration: J. Alcaraz et al., c protons, Physics Letters B 490, 27 (2000).
- [25] L.H. Smith et al., Astrophys. J. 180 987 (1973).
- [26] M. Ryan, J.F. Ormes, V.K. Balasubrahmanyam, Phys. Rev. Lett. 28 985 (1972).
- [27] JACEE Collaboration: K. Asakimori et al., Astrophys. J., 502, 278 (1998).
- [28] I.P. Ivanenko et al., Proc. 23rd ICRC, Calgary, 2, 17 (1993).
- [29] M. Ichimura et al., Phys. Rev. D 48, 1949 (1993).
- [30] P. Lipari, T. Stanev, and T.K. Gaisser, Phys. Rev. D58 (1998) 073003).
- [31] The Super-Kamiokande Collaboration: T. Futagami et al., Phys. Rev. Letters 82 (1999) 5194).
- [32] T.K. Gaisser and T. Stanev, Phys. Rev. D57 (1998) 1977).